Lab on a Chip

PAPER

View Article Online
View Journal | View Issue



Cite this: *Lab Chip*, 2020, **20**, 3461

# Scaling of deterministic lateral displacement devices to a single column of bumping obstacles

Weibin Liang, [ab] Robert H. Austin [ac] and James C. Sturm*[ab]

Received 3rd June 2020,
Accepted 23rd July 2020

DOI: 10.1039/d0lc00570c

rsc.li/loc

We describe a deterministic lateral displacement (DLD) for particle separation with only a single column of bumping features. The bifurcation of fluid streams at obstacles is not set by the "tilt" of columns with respect to macroscopic current flow, but rather by the fluidic resistances for lateral flow at each obstacle. With one column of 14 bumping features and corresponding inlet/outlet channels, the single-column DLD can separate particles with diameters of 4.8 μm and 9.9 μm at 30 μL min$^{-1}$, with an area of only 0.37 mm × 1.5 mm (0.55 mm$^2$). The large-cell output contains over 99% of the 9.9 μm particles and only 0.2% of the 4.8 m particles. The throughput per area of 54 μL min$^{-1}$ per mm$^2$ represents a 10× increase over previous selective harvesting reports for microfluidic devices in a similar particle size range.



## 1 Introduction

Cell separation for clinical applications, such as T cell harvesting for gene therapy,[1] requires high-throughput and a compact design for low cost. Microfluidic technologies for separating particles in 1 to 10 μm range can be classified into two types, "active" and "passive". The active technologies include dielectrophoretic,[2] magnetic,[3] acoustic,[4] thermophoretic[5] mechanisms, *etc.*; passive technologies include pinched flow, inertial focusing, hydrodynamic filtration, viscoelastic separation,[6] surface affinity,[7] and deterministic lateral displacement (DLD).[8] Active technologies are attractive because they are more configurable and/or tunable. For example, fluorescence-activated cell sorting *via* a traveling surface acoustic beam enables antigen-based on-chip cell sorting.[9] However, active approaches are also more complicated to implement than passive technologies, since the latter are based solely on the behavior of particles in flow patterns created by microstructures.

DLD technology has been widely studied and is attractive because of its simplicity, robustness and high-resolution.[10] It has been demonstrated over an extremely large range of particle sizes (over 1000×), with critical particle sizes for separation from exosomes at 20 nm[11] up to circulating tumor cells at 30 μm.[12] Because the physical mechanism is deterministic, not random like that of devices based on diffusion, the limit on the demonstrated resolving power of the device is at worst 1–2% of the particle size, or less than 20 nm for micron-sized particles.[8] This compares favorably to even non-microfluidic methods such as hydrodynamic chromatography and quasi-elastic laser light scattering, which can resolve particles in the micron range to an accuracy of 15% and 3%, respectively.[13,14] Furthermore, a given device is not restricted to a certain input pressure or a narrow range of flow rates, as are some devices such as those based on inertial effects.[15]

All microfluidic technologies, by their "micro" nature, have throughput limitations, especially regarding throughput. Towards this goal of high throughput, in this paper we show how the deterministic lateral displacement (DLD) device can

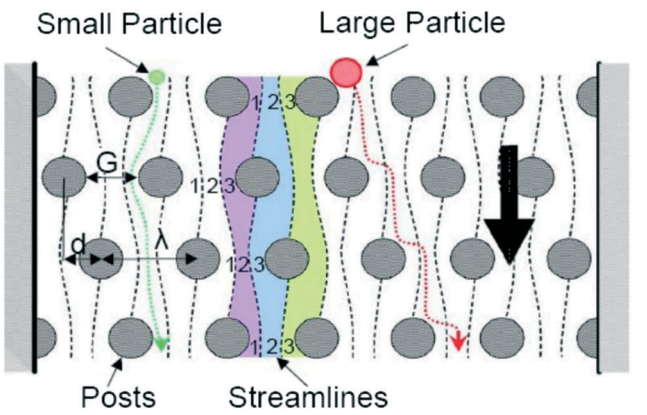


**Fig. 1** Schematic of a conventional DLD array.[16] The black arrow represents the average macroscopic flow direction, and the tilt angle ($\varepsilon = d/\lambda$) of the post columns is 1/3 in this figure. The regions 1, 2 and 3 with different colours shows the flow segmentation which determines the critical particle diameter. A small particle (green) flows along the streamtube while a large particle (red) bumps along the posts and migrates toward the right.

[a] *Princeton Institute for Science and Technology of Materials (PRISM), Princeton, New Jersey 08544, USA. E-mail: weibinl@princeton.edu*
[b] *Department of Electrical Engineering, Princeton University, Princeton, New Jersey 08544, USA*
[c] *Department of Physics, Princeton University, Princeton, New Jersey 08544, USA*

be scaled down to an extremely small size while maintaining a high flow rate. With a single column of obstacles, a throughput of over 50 μL $min^{-1}$ per $mm^2$ is demonstrated.

Deterministic lateral displacement is a technique for particle separation based on flow segmentation.[8,16] Traditionally, a particle-containing fluid, confined by walls, flows vertically through an array of post obstacles, whose vertical axis is "tilted" with respect to the macroscopic average flow direction (Fig. 1). A small particle flows along a streamtube towards a small-particle collection outlet, while a particle larger than a critical diameter "bumps" off successive posts from one streamtube to adjacent one, a process that repeats at each row. It ends up in a "large-particle" collection outlet at the bottom right of the device.

The critical diameter of the conventional DLD array depends on the width of the streamtube adjacent to the bumping surface, and can be experimentally adjusted by the gap size G between the posts and tilt angle $\varepsilon$.[17] A bulk array with posts and mirrored layout benefits from the uniform flow within the array (except for the boundaries). This conventional design has been widely used for particles and cells sorting from 20 nm[11] to 30 μm[12] because of its stable performance.[18,19] However, the conventional design suffers from limited throughput per area. Large particles migrate towards the collection outlet after bumping through $1/\varepsilon$ rows of posts for each column of obstacles it has to cross (a "unit cell"). A typical $\varepsilon$ of 1/20, implies 20 rows per column. To increase throughput with fixed fluid velocity, the number of columns is increased. To collect large particles that enter the

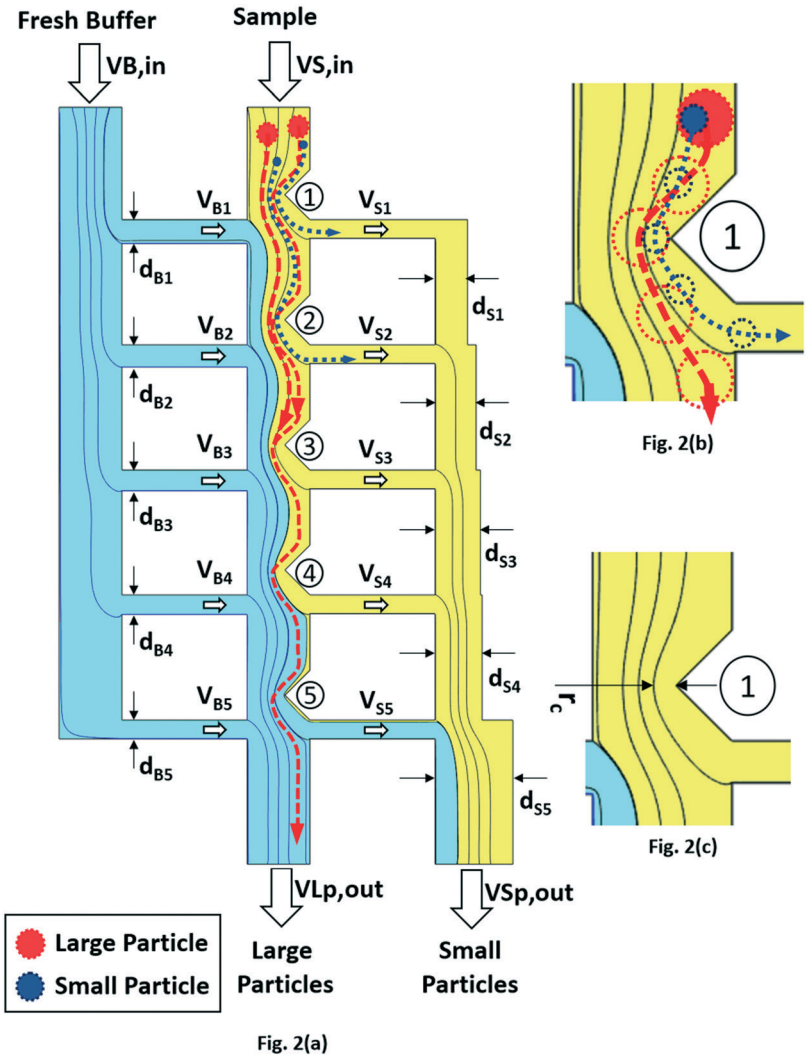


Fig. 2 Schematic of single-column DLD device. The overall schematic of the single-column DLD device with 5 rows of bumping obstacles. The thin black lines represent streamlines. The particle-containing "Sample" fluid (yellow) and a buffer without particles (blue) enter from the top. By the end (bottom) of the device, in the central column the original fluid is completely replaced by the fresh buffer, small particles (blue circles) flow along the streamtubes (dashed blue lines) and exit the device from the small particle outlet on the bottom. The red circles represent the particles larger than the critical diameter and the red dashed line with arrow shows their trajectories. All bumping occurs on the protruding obstacles in the central column. Large particles in the streamtube adjacent to the obstacles are "displaced" by the obstacles and remain in the central column, exiting the device from the large particle outlet.

 

top of the array far from the large particle collection outlet on the bottom right, the number of columns grows as the number of rows. (For example, a DLD array with 5 columns, each requiring 20 rows of posts, requires at least 5 × 20 rows of posts; a DLD array with 10 columns of 20 rows requires at least 10 × 20 rows). Thus the device area increases as the square of the throughput, and throughput per area decreases as the throughput increases. Further, at least half (the lower left half) of the entire DLD array is "idle" since no large particles are bumping within this region.

Here we propose a new approach to shrink the DLD while maintaining its fundamental concept of large particles repeatedly bumping off of multiple rows of obstacles. This new design consists of only one column of bumping obstacles. Fig. 2(a) shows its schematic. The mechanism of size-based particle separation is the same as the conventional DLD array, but the lateral displacement of particles, colloquially referred to as "bumping," only occurs in the central column. While bumping is a complex process, for the purposes of illustration we assume a particle follows the streamtube where its center lies, and that the particle is a rigid sphere. As in the conventional DLD, small particles (blue circles in the figure) follow the fluid flow, hence coming out at the bottom right $VB_{,in}$.

Note in the central column, at each row an obstacle to flow protrudes into the column from the right (Fig. 2b). When the streamtube adjacent to the right wall becomes narrow near an obstacle (Fig. 2b), a particle larger than a critical diameter can no longer "fit" into the streamtube adjacent the obstacle wall, and "bumps" off the wall so that its center falls into the adjacent streamtube (Fig. 2c). The large particle then follows the path of the new streamtube. Due to fluid from the central channel exiting to the small particle outlet channel, at the next bumping point, this new streamtube becomes the one adjacent to the bumping point, and the process of Fig. 2(b) repeats. Thus large particles remain in the central channel to leave in the "large particle" outlet and small ones leave. Thus the device is based on the same principle as the conventional deterministic lateral displacement device of Fig. 1. However, in the device of this work there is only one particle-carrying channel in the vertical dimension, and only one "unit cell" of rows, leading to its extremely small size. After the final bump, all the original buffer exits the middle channel which indicates the complete replacement of buffer and depletion of small particles from the middle channel (in the schematic of Fig. 2, small and large particles should already be completely separated after the forth obstacle, so the fifth is there only for a "safety factor" in case a particle "misses a bump" due to some non-ideality). The critical diameter determining which particles bump can be qualitatively determined by the distance from the post and the streamline that determines the flow segmentation (Fig. 2(b) and (c)). The critical diameter $d_c$ in Fig. 2(b) can be estimated by $d_c = 2r_c$, where $r_c$ is the distance from the post and the streamline that determines the flow segmentation. Instead of tuning the segmentation of flow and thus critical particle size by tilt angle $\varepsilon$ of the post columns with respect to the macroscopic fluid flow as in a conventional DLD array, in the new design the flow segmentation is controlled by the lateral fluid flows into ($V_{B1}$–$V_{B5}$) and out of ($V_{S1}$–$V_{S5}$) of the central channel. These in turn are set by the fluidic resistances of central vertical channel compared to that of the flow paths of buffer coming into the central channel from the left and of fluid leaving the central channel flowing through the right horizontal channel. For example, larger $d_{Bi}$'s and larger $d_{Si}$'s allow a larger lateral flows compared to the vertical flow and thus increase the critical diameter. To achieve the same critical particle size in each row, the device was designed for identical flow patterns in the central channel at each obstacle. Since a portion of the sample containing-fluid exits the central vertical channel at each row, a certain amount of fresh buffer needs to be injected to the central channel from the left. This was done by adjusting $d_{Bi}$ ($i$ = 1 to 5) and $d_{Si}$ at each row so that $V_{Bi} = V_{Si}$. For this design choice, this implies that the volumetric flow rate of the output containing large particles (*i.e.* above the critical size), $VLp_{,out}$, is equal to that for small particles $VSp_{,out}$.

In conventional DLD devices, both theory and data show the critical separation size scales linearly with lateral device dimensions.[20] By reducing the gap size to 25–235 nm, DLD arrays have successfully separated exosomes and colloids down to 20 nm in size.[11] Because the single-column DLD is based on the same flow segmentation theory as conventional DLD devices, we expect its critical size to similarly scale down as well.

## 2 Materials and methods

### 2.1 Device design

Fig. 3 displays the single-column DLD device with a critical diameter of 8 μm. It consists of 14 bumping points (analogous to rows in a conventional device). The width of the middle channel is 50 μm, the height of each triangle bump (Fig. 3, $h$) is 20 μm, and the width of the small channels which connect the centre channel to the small particle collection output is 15 μm. The total width of this design (not including the inlet/outlet ports) is 369 μm, and the total length is 1505 μm. The channel depth is 12 μm over the entire device. The width of the small particle collection outlet (dS$i$) and the fresh buffer inlet channels (dB$i$) were designed with 2-D numerical simulation of the flow patterns using MATLAB and COMSOL Multiphysics 5.3.

To design the device, we first decided on the obstacle shape and 30 μm gap width, and then used computational modelling of fluid flow (COMSOL Multiphysics 5.3) to design the fluidic resistor channels widths. If the narrowest width of the diverging streamtube at an obstacle was smaller (larger) than the target (the critical particle radius), as illustrated in Fig. 2(c) and described above, we reduced (increased) the fluidic resistance of the horizontal channel to the right of the obstacle to adjust the flow segmentation. This was iterated

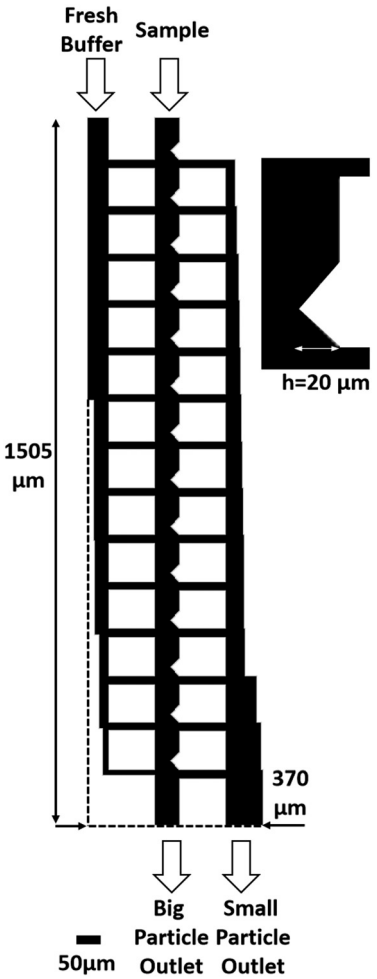


Fig. 3 Actual design of the single column DLD device used in the experiment. It consists of 14 bumping obstacles. The entire device (not including the inlet/outlet ports) measured 1.5 mm long by 0.37 mm wide with a uniform channel depth of 12 μm.

on all obstacles until the critical particle diameters were all within 0.1 μm of the target. The shape of the obstacle (such as round *vs.* a triangle) does affect the width of the adjacent streamtube and hence the critical size, as studied in conventional DLD's.[21,22] This effect was thus implicitly included in our modelling, although the shape of the triangular obstacle was not varied in this work. Further, this initial design did not take into account second-order effects, such as the affect of the shape of the obstacle on any potential particle deformation.[23,24]

### 2.2 Device fabrication and operation

The device was fabricated in silicon wafer using standard microfabrication techniques. Deep reactive ion etching (DRIE) was used to etch the channel. Etching mask was formed on the silicon wafer using standard photolithography (Heidelberg DWL 66+) with AZ1505 photoresist (AZ Electronic Materials, USA) and AZ 300 MIF developer. A SAMCO RIE800iPB reactive-ion etcher was used to perform a 12 μm deep etching. Inlets and outlets were 300 μm through-wafer holes created by laser drill. The device was sealed with a polyolefin sealing tape (9795RR, 3M, USA). The device was mounted to a polycarbonate jig with stainless steel ports. Two syringe pumps (Fusion 100T) were used to inject the buffer and sample.

An inverted microscope (Nikon Eclipse TE2000-5) was used to image the movement of particles and flow pattern within the device, with a blue-LED light (as the excitation source) with a fluorescence filter set (FITC, 467–498 nm excitation, 513–556 nm emission). Images and movies were captured with a 4× Nikon Plan Fluor objective (0.13 NA and 1.2 mm WD)/10× Nikon Plan objective (0.25 NA and 10.5 mm WD) using a Cannon camera (Cannon Eos 5D) and DSLR Remote Pro software by Breeze Systems.

The device was flushed with 0.2% Pluronic F108 surfactant in DI water for 5 minutes. The buffer and sample were injected into the chips by two syringe pumps at 30 μL $min^{-1}$ and two centrifuge tubes were used to collect the waste and the product. Finally, a hemocytometer (SKC, Inc. C-Chip Disposable hemocytometers) was used to count the particles in the product and the waste and calculate the recovery rate (particles in the product divided by the sum of particles in the product and waste).

### 2.3 Preparation of experimental samples

The fluorescent particles (Thermo Scientific™ Fluoro-Max dye green aqueous fluorescent polymer microsphere, 9.9 μm, 10 mL; Thermo Scientific™ Fluoro-Max dye green aqueous fluorescent polymer microsphere, 4.8 μm, 10 mL; Bang Laboratories, Inc. Green fluorescent polymer particles, 7.32 μm, 1 mL; Duke standards green fluorescent polymer microsphere, 0.088 μm, 15 mL) are diluted in 0.2% Pluronic F108 surfactant in DI water (particle concentration 1500 to 5000 microparticles per microliter for 9.9 μm/7.32 μm/4.8 μm microparticles; more than 10 000 particles per microliters for 0.088 μm microparticles).

## 3 Results and discussion

### 3.1 Experiment results

To confirm the basic fluid flows in the device, in a first experiment the buffer input and the particle input flows were spiked separately, one at a time (without large beads) with 0.088 μm fluorescent polystyrene microparticles. The small size insures that bumping effects on the particles are negligible. They have an estimated diffusion coefficient of $3 \times 10^{-12}$ $m^2$ $s^{-1}$. Given flow rates of 30 μL $min^{-1}$ (corresponding to a flow speed of approximate 1 m $s^{-1}$) and a device length of 1.5 mm, the estimated diffusion length of the particles during their time in the device is approximately 0.05 μm. Because this is much smaller than the widths of the channels in the device, the fluorescence of the particles should be a good marker of the fluid flows. Fig. 4(a) is a false-color overlay of 2 images, one with the sample input spiked with the fluorescent microparticles and one with the buffer input

 

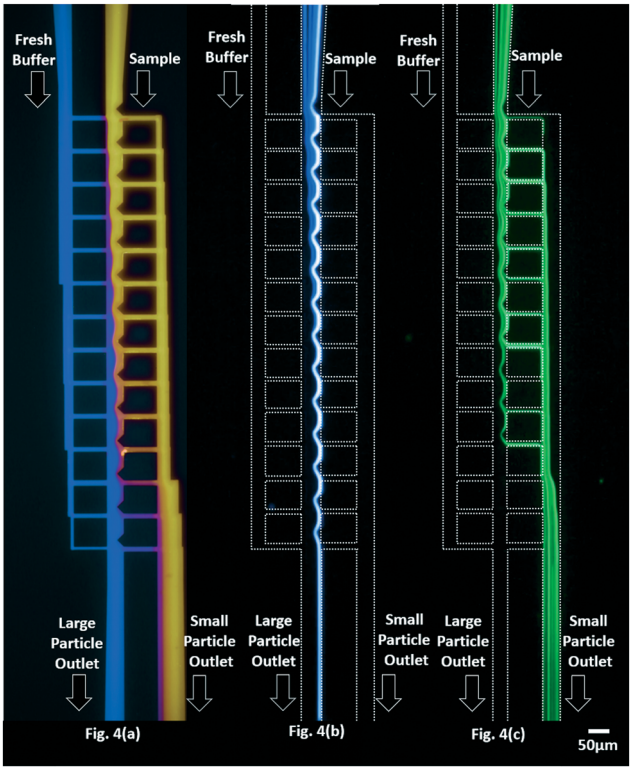


**Fig. 4** Fluorescent images showing fluid flow patterns and microparticle trajectories. The dotted lines indicate the approximate channel locations. (a): Flow pattern (overlay figures), exposure time: 1.3 s; (b) 9.9 μm microparticle trajectories, exposure time 1/30 s; (c) 4.8 μm microparticle trajectories, exposure time 1/30 s.

spiked with the microparticles. The image of Fig. 4(a) confirms the flow patterns described in the device description of Fig. 2. At the top of the device, the flow in the central channel consists entirely of the sample input, but by the end of the device, it has been entirely replaced with the buffer input.

We then tested the device with fluorescent polystyrene beads in the input, with diameters of 4.8 μm and 9.9 μm. The bead density was in the order of 1000 particles per micro liter. The flow rates of the sample input (containing the beads) and the buffer input were both set at 30 μL $s^{-1}$ by syringe pumps. Fig. 4(b) and (c) are time lapse fluorescent images of the movement of beads in the device with diameters of 4.8 μm and 9.9 μm, respectively. Over the exposure time of 0.03 s, approximately 20 particles flowed through the device. Fig. 4(a) and (b) clearly shows that this single-column DLD can separate the 4.8 μm and 9.9 μm particles, as expected, based on the designed critical size of 8.0 μm (the particles used in the experiments emit green fluorescence under excitation and the blue color of 9.9 μm particles is pseudocolor).

Note that the particles cover the complete width of the sample input channel to the device. Unlike some particle separation methods,[31–34] no pre-focusing of the particles to the center of the input channel (or elsewhere) is required. This contributes to device simplicity and removes restrictions

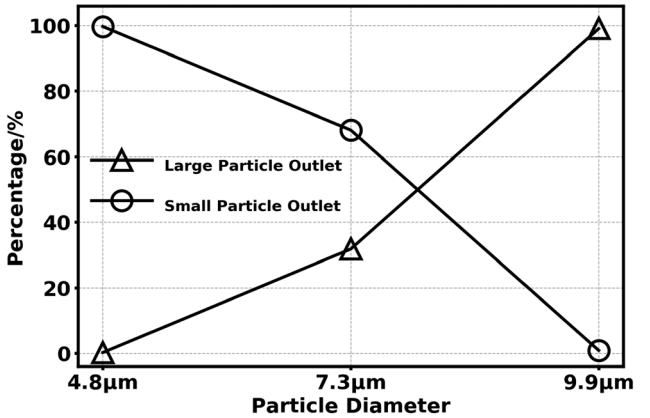


**Fig. 5** Experimental results showing the fraction of the input particles in the large and small particle output streams of 4.8 μm, 7.3 μm, and 9.9 μm microparticles.

on input flow rate, for example. Fig. 5 summarizes the separation ability of the device for input particles with diameters of 4.8 μm, 7.3 μm, and 9.9 μm. The flow rates of the buffer input and of the sample (particle-containing) input were both 30 μL $min^{-1}$. A sample volume of 300 μL was processed in 10 minutes. The single-column DLD device sent 99.9% of the 9.9 μm microparticles to the large particle output, and only 0.2% of the 4.8 μm beads. Conversely the small particle output had 99.9% of the 4.8 μm beads and only 0.2% of the 9.9 μm beads. The device sent 32% of the 7.3 μm particles to the large and 68% to the small particle output. Since 7.3 μm is very close to the designed critical diameter of 8 μm (the partial separation of such 7.3 μm particles is expected). The percentage of particles in the large particle outlet/small particle outlet is calculated by dividing the number of particles in the large particle outlet/small particle outlet by the sum of the number of particles in the large and small particle outlets.

### 3.2 Discussion

The motivation for this work was a high throughput per unit area. While one device has small throughput due to only one column, building multiple devices in parallel would lead to a throughput increasing linearly with area, not as the square as with a single large area. Table 1 shows some comparisons of throughput per device area shown in this work (area not counting inlet and outlet regions beyond that of Fig. 3), along with that of the other reported size-based particle separation approaches. The work of this paper has a throughput/area over one order of magnitude larger than that reported in prior work for large particle sizes of 13.6 μm and below,[25–28] and 3× larger than that for large particle sizes of 17 and 25 μm.[29,30] A scaled-down version of a conventional bump array with one or two columns of posts (not with the individually tailored fluid resistors at each obstacle in a central channel as in this work) had a demonstrated throughput/area 100× lower than that demonstrated here.[35]

Table 1 Comparison between different designs

| Ref. | Design | Small particle | Big particle | Throughput (μL min$^{-1}$) | Device area (mm$^2$) | Throughput per area (μL min$^{-1}$ mm$^{-2}$) |
|---|---|---|---|---|---|---|
| M. Pødenphant[25] | Pinched flow | WBC (7.1 μm) | LS174T (13.6 μm) | 0.17 | 1 | 0.17 |
| A. Al-Halhouli[26] | Inertial spiral channel | Beads (2 μm) | Beads (5 μm) | 1000 | 445 | 2.3 |
| B. R. Mutlu[27] | Non-equil. inertial array | RBC (<7 μm) | WBC (10 μm) | 60 | 18 | 3.3 |
| J. D'Silva[28] | High-throughput DLD | RBC | WBC | 360 | 90 | 4 |
| J. D'Silva[29] | Clotting inhibition DLD | RBC | PC3 (17 μm) | 1470 | 85 | 17.3 |
| Z. Liu[30] | Rapid cancer cell isolation DLD | RBC | MCF-7 (15–25 μm) | 2000 | 122.5 | 16.3 |
| L. Weibin | This work | Beads (4.8 μm) | Beads (9.9 μm) | 30 | 0.56 | 54 |

The small number of rows may have other advantages. For example, since large particles bump at each row, the single-column design may lead to less cell damage from the bumping process. Fewer rows (and thus less time in the array) may also lead to less clogging.[29]

The device presented here has successfully separated beads processing input quantities up to 1 ml with no trace of clogging. It is well known that processing blood in DLD devices can lead to clogging due to cell sticking and clotting issues. With appropriate anti-clogging additives and pre-filtering (to remove large incoming cell clumps),[36] 50 mL of input can be processed in a conventional device with a 0.6 mm-wide array.[37] For our device with an input width of 50 μm, this would translate to a throughput of 4 mL without clogging.

No effort was made in this first demonstration to concentrate the large particles which were harvested. By tapping off only a small portion of the "large particle" output, some degree of concentration should be straightforward. Related, we also note that in principle the "buffer input" (see Fig. 2) could be greatly reduced or even eliminated by sequentially narrowing the central column after each obstacle. This would also lead to concentration of the large particles. In this demonstration we elected not to do this, keeping the central vertical channel wide to reduce the possibility of clogging.

The present design separates particles into two streams. In conventional DLD's, others have used multiple obstacle arrays in series, each with its own critical size, to separate particles into multiple streams based on size, not just two.[38,39] In principle, the single-column approach should be amenable to such an approach as well.

Achieving throughput in the milliliters per minute range using the single-column devices would require running multiple devices in parallel; at the same device flow rate, 3 mL min$^{-1}$ would require 100 of the present devices. To reduce the complexity of tubing and external connections, integrating devices together on a common substrate with a small number of external connections would be desirable. Assuming the connections require, on average, the same area as the devices, 3 mL min$^{-1}$ implies an area of 120 mm$^2$.

## 4 Conclusions

In this paper we have demonstrated an approach to scale the deterministic lateral displacement concept for particle fractionation to a single column of bumping obstacles. The very small device area led to a very high throughput/area, which is 10× larger than that in previous work for particle separation in the 5–10 μm range. Thus the device is potentially attractive for harvesting leukocytes from blood and other applications.

## Conflicts of interest

There are no conflicts to declare.

## Acknowledgements

This work was funded by NIH (project number 4R42CA228616-02).

## Notes and references

1 R. Campos-González, A. M. Skelley, K. Gandhi, D. W. Inglis, J. C. Sturm, C. I. Civin and T. Ward, *SLAS Technol.*, 2018, **23**, 338–351.
2 K. Zhao, Larasati, B. P. Duncker and D. Li, *Anal. Chem.*, 2019, **91**, 6304–6314.
3 O. Sarigil, M. Anil-Inevi, E. Yilmaz, G. Mese, H. C. Tekin and E. Ozcivici, *Analyst*, 2019, **144**, 2942–2953.
4 Y. Gu, C. Chen, Z. Wang, P.-H. Huang, H. Fu, L. Wang, M. Wu, Y. Chen, T. Gao, J. Gong, J. Kwun, G. M. Arepally and T. J. Huang, *Lab Chip*, 2019, **19**, 394–402.
5 D. Vigolo, R. Rusconi, H. A. Stone and R. Piazza, *Soft Matter*, 2010, **6**, 3489–3493.
6 X. Lu, C. Liu, G. Hu and X. Xuan, *J. Colloid Interface Sci.*, 2017, **500**, 182–201.
7 S. Nagrath, L. V. Sequist, S. Maheswaran, D. W. Bell, D. Irimia, L. Ulkus, M. R. Smith, E. L. Kwak, S. Digumarthy, A. Muzikansky, P. Ryan, U. J. Balis, R. G. Tompkins, D. A. Haber and M. Toner, *Nature*, 2007, **450**, 1235–1239.
8 L. R. Huang, E. C. Cox, R. H. Austin and J. C. Sturm, *Science*, 2004, **304**, 987–990.
9 Z. Ma, Y. Zhou, D. J. Collins and Y. Ai, *Lab Chip*, 2017, **17**, 3176–3185.
10 T. Salafi, Y. Zhang and Y. Zhang, *Nano-Micro Lett.*, 2019, **11**, 77.
11 B. H. Wunsch, J. T. Smith, S. M. Gifford, C. Wang, M. Brink, R. L. Bruce, R. H. Austin, G. Stolovitzky and Y. Astier, *Nat. Nanotechnol.*, 2016, **11**, 936–940.

 

12 S. H. Au, J. Edd, A. E. Stoddard, K. H. K. Wong, F. Fachin, S. Maheswaran, D. A. Haber, S. L. Stott, R. Kapur and M. Toner, *Sci. Rep.*, 2017, **7**, 2433.
13 M. T. Blom, E. Chmela, R. E. Oosterbroek, R. Tijssen and A. van den Berg, *Anal. Chem.*, 2003, **75**, 6761–6768.
14 D. B. Sattelle, A. L. Obaid and B. M. Salzberg, *Biochem. Soc. Trans.*, 1991, **19**, 501–501.
15 J. Zhang, S. Yan, D. Yuan, G. Alici, N.-T. Nguyen, M. E. Warkiani and W. Li, *Lab Chip*, 2016, **16**, 10–34.
16 J. A. Davis, D. W. Inglis, K. J. Morton, D. A. Lawrence, L. R. Huang, S. Y. Chou, J. C. Sturm and R. H. Austin, *Proc. Natl. Acad. Sci. U. S. A.*, 2006, **103**, 14779–14784.
17 D. W. Inglis, J. A. Davis, R. H. Austin and J. C. Sturm, *Lab Chip*, 2006, **6**, 655–658.
18 F. Fachin, P. Spuhler, J. M. Martel-Foley, J. F. Edd, T. A. Barber, J. Walsh, M. Karabacak, V. Pai, M. Yu, K. Smith, H. Hwang, J. Yang, S. Shah, R. Yarmush, L. V. Sequist, S. L. Stott, S. Maheswaran, D. A. Haber, R. Kapur and M. Toner, *Sci. Rep.*, 2017, **7**, 10936.
19 Z. Liu, F. Huang, J. Du, W. Shu, H. Feng, X. Xu and Y. Chen, *Biomicrofluidics*, 2013, **7**, 011801.
20 D. W. Inglis, J. A. Davis, R. H. Austin and J. C. Sturm, *Lab Chip*, 2006, **6**, 655.
21 K. Loutherback, K. S. Chou, J. Newman, J. Puchalla, R. H. Austin and J. C. Sturm, *Microfluid. Nanofluid.*, 2010, **9**, 1143–1149.
22 J. Wei, H. Song, Z. Shen, Y. He, X. Xu, Y. Zhang and B. N. Li, *IEEE Trans. NanoBiosci.*, 2015, **14**, 660–667.
23 T. Krüger, D. Holmes and P. V. Coveney, *Biomicrofluidics*, 2014, **8**, 054114.
24 Z. Zhang, E. Henry, G. Gompper and D. A. Fedosov, *J. Chem. Phys.*, 2015, **143**, 243145.
25 M. Pødenphant, N. Ashley, K. Koprowska, K. U. Mir, M. Zalkovskij, B. Bilenberg, W. Bodmer, A. Kristensen and R. Marie, *Lab Chip*, 2015, **15**, 4598–4606.
26 A. Al-Halhouli, A. Albagdady and A. Dietzel, *RSC Adv.*, 2019, **9**, 41970–41976.
27 B. R. Mutlu, K. C. Smith, J. F. Edd, P. Nadar, M. Dlamini, R. Kapur and M. Toner, *Sci. Rep.*, 2017, **7**, 9915.
28 J. D'Silva, *Ph.D. Thesis*, Princeton University, 2016.
29 J. D'Silva, R. H. Austin and J. C. Sturm, *Lab Chip*, 2015, **15**, 2240–2247.
30 Z. Liu, F. Huang, J. Du, W. Shu, H. Feng, X. Xu and Y. Chen, *Biomicrofluidics*, 2013, **7**, 011801.
31 Z. Wu, Y. Chen, M. Wang and A. J. Chung, *Lab Chip*, 2016, **16**, 532–542.
32 J. Zhang, S. Yan, R. Sluyter, W. Li, G. Alici and N.-T. Nguyen, *Sci. Rep.*, 2014, **4**, 4527.
33 M. Wu, A. Ozcelik, J. Rufo, Z. Wang, R. Fang and T. Jun Huang, *Microsyst. Nanoeng.*, 2019, **5**, 32.
34 J. Nam, W. S. Jang, D. H. Hong and C. S. Lim, *Sci. Rep.*, 2019, **9**, 3067.
35 L. Huang, System and method for particle filtration, *U.S. pat.* 8,679,751 B2, 2014.
36 D. W. Inglis, M. Lord and R. E. Nordon, *J. Micromech. Microeng.*, 2011, **21**, 054024.
37 Z. Wu, Y. Chen, M. Wang and A. J. Chung, *Lab Chip*, 2016, **16**, 532–542.
38 E. Pariset, C. Parent, Y. Fouillet, B. François, N. Verplanck, F. Revol-Cavalier, A. Thuaire and V. Agache, *Sci. Rep.*, 2018, **8**, 17762.
39 J. A. Davis, D. W. Inglis, K. J. Morton, D. A. Lawrence, L. R. Huang, S. Y. Chou, J. C. Sturm and R. H. Austin, *Proc. Natl. Acad. Sci. U. S. A.*, 2006, **103**, 14779–14784.